A four dimensional quantum scattering study of the $Cl+CH_4 \rightleftharpoons HCl+CH_3$ reaction via spectral transform iteration

Hua-Gen Yu and Gunnar Nyman[a)]
Department of Chemistry, Physical Chemistry, Göteborg University, S-412 96 Göteborg, Sweden

(Received 8 December 1998; accepted 12 January 1999)

We present a quantum dynamics study of the $Cl+CH_4 \rightleftharpoons HCl+CH_3$ reaction using a four-dimensional rotating bond umbrella (RBU) model. A semiempirical potential energy surface is employed, where the zero point energy of the modes not explicitly treated in the RBU calculations is approximately included. The potential gives a vibrationally adiabatic ground state barrier height of 3.48 kcal/mol. The calculations have been performed in hypercylindrical coordinates using a log-derivative method. A single sector hyperspherical projection method has been developed for applying boundary conditions. A guided spectral transform (GST) Krylov subspace method has been constructed to find the eigenstates of the coupling matrix appearing in the coupled channel equations. The results show that the product methyl is rotationally cold for the forward reaction. A pronounced tunneling effect on the rate constants was obtained. The calculated thermal rate constants are 12%–45% smaller than the experimental results over the temperature range 200–800 K for the $Cl+CH_4 \rightleftharpoons HCl+CH_3$ reaction. State-to-state differential cross sections have been studied at a kinetic energy of 0.159 eV. A detailed comparison with experimental measurements is made.
 [S0021-9606(99)01114-9]

I. INTRODUCTION

Since Schatz and Kuppermann[1] carried out the first converged quantum dynamics computations of cross sections for the $H+H_2$ reaction in 1976, quantum reactive scattering theory has progressed substantially. Rigorous quantum dynamical calculations have been extended to reactions involving four atoms.[2–7] The first calculations for a collinear four-atom chemical reaction $H+HCN \rightarrow H_2+CN$ were performed independently by Sun and Bowman[8] and Brooks and Clary.[9] Then, Clary[10] developed the rotating bond approximation (RBA) and applied it to the reaction $OH+H_2 \rightarrow H_2O+H$ with nonlinear geometry. In its fullest form, the RBA explicitly accounts for all three vibrational modes and the rotational degree of freedom of the unbroken bond.[10–12]

The RBA has been applied to many other tetraatomic and polyatomic reactions.[2,11,13,14] Recently, Clary and coworkers have also performed planar[15] and five-dimensional[3] quantum reaction scattering calculations on $OH+H_2 \rightarrow H_2O+H$. Bowman and Wang have developed an adiabatic treatment of the bending vibrations[16] and applied it to the nonlinear reaction $OH+H_2 \rightarrow H_2O+H$ (Ref. 16) as well as the $H+C_2H_2 \rightarrow H_2+C_2H$ reaction.[17] For general four-atom chemical reactions, various theories have also been developed by other groups.[4–7,18,19]

In coupled channel quantum scattering calculations, hyperspherical coordinates have been commonly used. The hyperspherical coordinates describe all the possible reaction channels so that it becomes essentially equivalent to solve the reactive and nonreactive scattering problems. The whole *S* matrix is obtained in one propagation. However, in order to accurately calculate the *S* matrix, one should project the solutions in hyperspherical coordinates onto the asymptotic ones in Jacobi coordinates. The general way is to match the wave functions at a fixed scattering coordinate in Jacobi coordinates,[20–22] where the boundary conditions are applied. In practice, it is computationally cumbersome[23] to evaluate the elements of the matching matrices using the wavefunctions for several hyperradius (ρ) sectors.

To avoid this difficulty, Hayes, Pendergast and Walker[23] have recently developed an accurate hyperspherical projection method for their bending-corrected rotating linear model. This method only requires a single ρ-sector wave function. We have also used this projection method in the rotating line approximation (RLA) quantum scattering calculations on the $Cl+CH_4 \rightarrow HCl+CH_3$ reaction[24] and extended it to the 3D rotating line umbrella (RLU) model.[25] In this work, we further extend this technique to the 4D rotating bond umbrella (RBU) calculations, to be described in Sec. II.

We also note that an approximate approach is often used, where the boundary conditions are applied directly in hyperspherical coordinates.[10–12] Fortunately, quite accurate reaction probabilities can usually be obtained by averaging at large ρ, to largely cancel out the oscillating behaviour of the reaction probabilities as a function of ρ.[26] We also point out that the issue of accurately matching boundary conditions has been treated in detail by Pack and Parker in the context of an exact treatment of an atom–diatom reaction.[22]

The reaction $Cl+CH_4 \rightarrow HCl+CH_3$ plays an important role in the atmosphere. It has been the subject of extensive experimental and theoretical investigations (see Refs. 25,27,28, and references therein). Recently, we have performed reduced dimensionality quantum scattering calculations using the 2D RLA (Ref. 24) and 3D RLU (Ref. 25)

a)Electronic mail: nyman@phc.chalmers.se

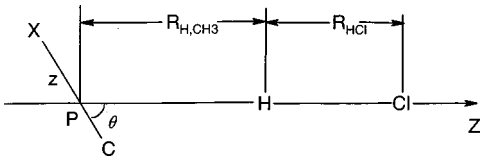

FIG. 1. Coordinates of the four dimensional rotating bond umbrella (RBU) model for the $Cl+CH_4 \rightleftharpoons HCl+CH_3$ reaction. X represents the pseudoatom with the mass $3m_H$ and is located at the center of mass of the three hydrogens in the CH_3 moiety. P is the CX center of mass.

models, obtaining quite good agreement with the experimental results. In the present work, some effects of nonlinear geometries and including one rotational degree of freedom of CH_3 are investigated.

In Sec. II we present a description of the 4D RBU model for the $Cl+CH_4 \rightleftharpoons HCl+CH_3$ reaction. The reduced dimensionality Hamiltonian in both hypercylindrical and Jacobi coordinates is defined. A concise derivation of formulas for the hyperspherical projection method is given. A guided spectral transform Krylov subspace iteration method is also described, which is followed by the evaluation of the surface Hamiltonian. The potential energy surface and numerical aspects are given in Sec. III, while results and discussion are presented in Sec. IV. Conclusions are found in Sec. V.

II. THEORY

A. Hamiltonian and coupled channel equations

The RBU model can be viewed as an extension of our 3D RLU model for the reaction $Cl+CH_4 \rightleftharpoons HCl+CH_3$ and is obtained by additionally including a rotational degree of freedom of the CH_3 moiety. The model treats the reaction as a four-atom system, $Cl+HCX \rightleftharpoons HCl+CX$, where X has the mass of three hydrogen atoms and is located at their centre of mass. As in the RBA developed by Clary,[10] the Cl and H atoms and the centre of mass of CX moves collinearly. The pseudodiatom CX approximately simulates the umbrella motion, where the three hydrogens in CH_3 move in phase with a fixed C–H bond length, $r_e = 2.052\,24$ a.u. For the rotation of CH_3, as a rigid body around the CX axis (''helicopter motion''), the potential energy is minimized as a function of the dynamical variables.

The RBU model includes four internal physical motions; the H–C and H–Cl reactive bond stretches, the umbrella type mode of the CH_3/CH_4 fragments, and a rotational mode of CH_3 which becomes a bending mode in CH_4. This 4D RBU model can also in essence be viewed as an extension of the RBA if one considers the umbrella mode as a vibrational motion of the unbroken bond and treats it explicitly in the dynamical calculation. The umbrella motion, however, is a large amplitude motion rather than a ''spectator'' bond. Thus, the umbrella vibrational frequency can change substantially along the reaction path so that it may play a role in the dynamics. The coordinates used are given in Fig. 1.

As described by Clary and Nyman,[10,11] the reduced dimensionality Hamiltonian can be expressed in hypercylindrical coordinates (ρ,φ,z,θ) as

$$\hat{H}(\rho,\varphi,z,\theta) = -\frac{\hbar^2}{2\mu}\left[\frac{1}{\rho^3}\frac{\partial}{\partial\rho}\rho^3\frac{\partial}{\partial\rho}+\frac{1}{\rho^2}\frac{\partial^2}{\partial\varphi^2}\right]-\frac{\hbar^2}{2\mu_z}\frac{\partial^2}{\partial z^2} + \frac{\hbar^2\hat{j}^2}{2I(z)}+\frac{\hbar^2}{2\mu\rho^2\sin^2\varphi}(\hat{j}^2-\Omega^2) + \frac{\hbar^2}{2\mu\rho^2}[J(J+1)-\Omega^2]+V(\rho,\varphi,z,\theta) \quad (1)$$

with the volume element for the internal variables

$$d\tau = \rho^3 d\rho d\varphi dz \sin\theta d\theta,$$

where

$$I(z) = m_H r_e^2(1-\cos\eta)+\frac{m_H m_C}{m_{CX}}r_e^2(1+2\cos\eta),$$

$$\cos\eta = \frac{3z^2-r_e^2}{2r_e^2},$$

$$\mu = \left[\frac{m_{Cl}m_H m_{CX}}{m_T}\right]^{1/2},$$

$$\mu_z = \frac{3m_C m_H}{m_{CX}},$$

$$m_T = m_{Cl}+m_H+m_{CX},$$

$$m_{CX} = m_C+3m_H,$$

and the rotational angular momentum operator is

$$\hat{j}^2 = -\frac{1}{\sin\theta}\frac{\partial}{\partial\theta}\sin\theta\frac{\partial}{\partial\theta}. \quad (2)$$

Here m_{Cl}, m_C, and m_H are the masses of the Cl, C, and H atoms, respectively. In Eq. (1), we have invoked the j_z-conserving approximation and the Z-axis of the body-fixed frame is along the H–Cl bond. Thus, both the total angular momentum J and Ω, the projection of J on the Z-axis, are good quantum numbers in the present model. V is the potential energy surface, which in the scattering calculations depends on the four internal coordinates (ρ,φ,z,θ). These coordinates are defined by the mass-scaled Jacobi coordinates $(R_\alpha, r_\alpha, R_\gamma, r_\gamma$, defined below) as

$$\begin{aligned} &\rho^2 = R_\alpha^2+r_\alpha^2 = R_\gamma^2+r_\gamma^2, \quad 0\leqslant\rho<\infty,\\ &\tan\varphi = r_\alpha/R_\alpha, \quad 0\leqslant\varphi\leqslant\varphi_{\max},\\ &z = z, \quad -r_e\leqslant z\leqslant r_e,\\ &\theta = \theta, \quad 0\leqslant\theta\leqslant\pi, \end{aligned} \quad (3)$$

with the maximum hyperangle

$$\varphi_{\max} = \tan^{-1}\left[\frac{m_H m_T}{m_{Cl}m_{CX}}\right]^{1/2}.$$

θ is the $\angle$HPC, where P is the CX center of mass, which in the product arrangement represents the methyl rotation, see Fig. 1. z is the position of X relative to C as shown in Fig. 1. This coordinate will be referred to as the umbrella coordinate. z and θ are unchanged by coordinate transformations between hypercylindrical and Jacobi coordinates. In this work, we use the symbols α and γ to label the reactant

$Cl+CH_4$ and product $HCl+CH_3$ channels, respectively. With the coordinate ranges given we have that $V(\rho,\phi,z,\theta)=V(\rho,\phi,-z,\pi-\theta)$. We have not used this pseudoinversion symmetry in the scattering calculations but accounted for it when evaluating the rate constants, as described later.

The mass-scaled Jacobi coordinates are given by

$$R_\alpha=C_\alpha^{-1}R_{\mathrm{Cl,CH_4}},\quad R_\gamma=C_\gamma^{-1}R_{\mathrm{HCl,CH_3}},$$

$$r_\alpha=C_\alpha R_{\mathrm{H,CH_3}},\quad r_\gamma=C_\gamma R_{\mathrm{HCl}},$$

$$C_\alpha=\left[\frac{m_T m_{\mathrm{H}} m_{\mathrm{CX}}}{m_{\mathrm{Cl}}(m_{\mathrm{H}}+m_{\mathrm{CX}})^2}\right]^{1/4},$$

$$C_\gamma=\left[\frac{m_T m_{\mathrm{Cl}} m_{\mathrm{H}}}{m_{\mathrm{CX}}(m_{\mathrm{Cl}}+m_{\mathrm{H}})^2}\right]^{1/4},$$

where $R_{\mathrm{Cl,CH_4}}$, $R_{\mathrm{H,CH_3}}$, $R_{\mathrm{HCl,CH_3}}$, and R_{HCl} are the distances of Cl to the CH_4 center of mass, of H to the CH_3 center of mass, of the HCl center of mass to the CH_3 center of mass and the HCl internuclear distance, respectively.

By using Eqs. (1) and (3), we can obtain the Hamiltonian in Jacobi coordinates for the α channel as

$$\begin{aligned}\hat{H}(R_\alpha,r_\alpha,z,\theta)=&-\frac{\hbar^2}{2\mu}\left[\frac{1}{\rho^2}\frac{\partial}{\partial R_\alpha}\rho^2\frac{\partial}{\partial R_\alpha}\right.\\&\left.+\frac{1}{\rho^2}\frac{\partial}{\partial r_\alpha}\rho^2\frac{\partial}{\partial r_\alpha}\right]-\frac{\hbar^2}{2\mu_z}\frac{\partial^2}{\partial z^2}+\frac{\hbar^2\hat{j}^2}{2I(z)}\\&+\frac{\hbar^2}{2\mu r_\alpha^2}(\hat{j}^2-\Omega^2)+\frac{\hbar^2}{2\mu\rho^2}\\&\times[J(J+1)-\Omega^2]+V,\\ d\tau=&\rho^2 dR_\alpha dr_\alpha dz\sin\theta d\theta,\end{aligned}\tag{4}$$

and for the γ channel as

$$\begin{aligned}\hat{H}(R_\gamma,r_\gamma,z,\theta)=&-\frac{\hbar^2}{2\mu}\left[\frac{1}{\rho^2}\frac{\partial}{\partial R_\gamma}\rho^2\frac{\partial}{\partial R_\gamma}+\frac{1}{\rho^2}\frac{\partial}{\partial r_\gamma}\rho^2\frac{\partial}{\partial r_\gamma}\right]\\&-\frac{\hbar^2}{2\mu_z}\frac{\partial^2}{\partial z^2}+\frac{\hbar^2\hat{j}^2}{2I(z)}+\frac{\hbar^2}{2\mu\rho^2\sin^2\varphi}\\&\times(\hat{j}^2-\Omega^2)+\frac{\hbar^2}{2\mu\rho^2}[J(J+1)-\Omega^2]+V,\\ d\tau=&\rho^2 dR_\gamma dr_\gamma dz\sin\theta d\theta.\end{aligned}\tag{5}$$

The hyperradius ρ is divided into L_S sectors i. Then, for all values of J and Ω, the functions $|\psi_m^{J\Omega}\rangle$ with initial quantum state m are expanded in the coupled channel form

$$\begin{aligned}|\psi_m^{J\Omega}(\rho,\varphi,z,\theta)\rangle=&\rho^{-3/2}\sum_{i=1}^{L_S}\sum_{n=1}^{N}h_{nm}(\rho;i,J,\Omega)\\&\times|H_n(\varphi,z,\theta;i,\Omega)\rangle\end{aligned}\tag{6}$$

in hyperspherical coordinates, or as

$$\begin{aligned}|\psi_m^{J\Omega\beta}(R_\beta,r_\beta,z,\theta)\rangle=&\rho^{-1}\sum_{n=1}^{N}f_{nm}^{\beta}(R_\beta;J,\Omega)\\&\times|F_n^{\beta}(r_\beta,z,\theta;\Omega)\rangle\end{aligned}\tag{7}$$

in Jacobi coordinates. Here, $|F_n^{\beta}(r_\beta,z,\theta;\Omega)\rangle$ are the vibrational/rotational states with eigenvalues $\mathcal{E}_n^{F^\beta}$ in the limit of large values of R_β for the $\beta(=\alpha,\gamma)$ channel. These states are determined by solving

$$\hat{H}^\alpha|F_n^\alpha(r_\alpha,z,\theta;\Omega)\rangle=\mathcal{E}_n^{F^\alpha}|F_n^\alpha(r_\alpha,z,\theta;\Omega)\rangle,\tag{8}$$

$$\begin{aligned}\hat{H}^\alpha=&-\frac{\hbar^2}{2\mu}\frac{\partial^2}{\partial r_\alpha^2}-\frac{\hbar^2}{2\mu_z}\frac{\partial^2}{\partial z^2}+\left(\frac{\hbar^2}{2I(z)}+\frac{\hbar^2}{2\mu r_\alpha^2}\right)\hat{j}^2\\&-\frac{\hbar^2}{2\mu r_\alpha^2}\Omega^2+V_F^\alpha(r_\alpha,z,\theta),\end{aligned}\tag{9}$$

$$V_F^\alpha(r_\alpha,z,\theta)=\lim_{R_{\alpha\to\infty}}V(\rho,\varphi,z,\theta),\tag{10}$$

$$\hat{H}^\gamma|F_n^\gamma(r_\gamma,z,\theta;\Omega)\rangle=\mathcal{E}_n^{F^\gamma}|F_n^\gamma(r_\gamma,z,\theta;\Omega)\rangle,\tag{11}$$

$$\begin{aligned}\hat{H}^\gamma=&-\frac{\hbar^2}{2\mu}\frac{\partial^2}{\partial r_\gamma^2}-\frac{\hbar^2}{2\mu_z}\frac{\partial^2}{\partial z^2}+\frac{\hbar^2}{2I(z)}\hat{j}^2+\frac{\hbar^2}{2\mu\rho^2\sin^2\varphi}\\&\times(\hat{j}^2-\Omega^2)+V_F^\gamma(r_\gamma,z,\theta),\end{aligned}\tag{12}$$

$$V_F^\gamma(r_\gamma,z,\theta)=\lim_{R_{\gamma\to\infty}}V(\rho,\varphi,z,\theta),\tag{13}$$

and are independent of J. In Eq. (6), $|H_n(\varphi,z,\theta;i,\Omega)\rangle$ are the eigenstates of the surface Hamiltonian $\hat{H}_S$ with the potential $V_H(\varphi,z,\theta;i)=V(\rho=\rho_i,\varphi,z,\theta)$ for fixed ρ, i.e.,

$$\hat{H}_S|H_n(\varphi,z,\theta;i,\Omega)\rangle=\mathcal{E}_n^H|H_n(\varphi,z,\theta;i,\Omega)\rangle,\tag{14}$$

$$\begin{aligned}\hat{H}_S=&-\frac{\hbar^2}{2\mu\rho_i^2}\frac{\partial^2}{\partial\varphi^2}-\frac{\hbar^2}{2\mu_z}\frac{\partial^2}{\partial z^2}+\frac{\hbar^2}{2I(z)}\hat{j}^2\\&+\frac{\hbar^2}{2\mu\rho_i^2\sin^2\varphi}(\hat{j}^2-\Omega^2)+V_H.\end{aligned}\tag{15}$$

The eigenstates are calculated by a Krylov subspace iteration method, which will be described below. The set of $\{|H_n(\varphi,z,\theta;i,\Omega)\rangle\}$ is also independent of J and orthogonal for a constant ρ_i, i.e.,

$$\langle H_{n'}(\varphi,z,\theta;i,\Omega)|H_n(\varphi,z,\theta;i,\Omega)\rangle=\delta_{n'n}.\tag{16}$$

By substituting the wave functions defined in Eqs. (6) and (7) into the time-independent Schrödinger equation $\hat{H}|\psi\rangle=E|\psi\rangle$, we obtain the coupled channel equations

$$\frac{d^2}{dR^2}f_{nm}^{\beta}(R_\beta;J,\Omega)+\sum_{n'=0}^{N}(\mathbf{D}_F^{\beta})_{nn'}f_{n'm}^{\beta}(R_\beta;J,\Omega)=0,\quad\beta=\alpha,\gamma,\tag{17}$$

$$\frac{d^2}{d\rho^2}h_{nm}(\rho;i,J,\Omega)+\sum_{n'=0}^{N}(\mathbf{D}_H)_{nn'}h_{n'm}(\rho;i,J,\Omega)=0,\tag{18}$$

where the coupling matrices have elements

$$(\mathbf{D}_F^{\alpha})_{nn'} = -\frac{2\mu}{\hbar^2}\langle F_n^{\alpha}|\hat{H}^{\alpha}+\frac{\hbar^2}{2\mu\rho^2}[J(J+1)-\Omega^2+1]-E|F_{n'}^{\alpha}\rangle,$$

$$(\mathbf{D}_F^{\gamma})_{nn'} = -\frac{2\mu}{\hbar^2}\langle F_n^{\gamma}|\hat{H}^{\gamma}+\frac{\hbar^2}{2\mu\rho^2}[J(J+1)-\Omega^2+1]-E|F_{n'}^{\gamma}\rangle, \tag{19}$$

$$(\mathbf{D}_H)_{nn'} = -\frac{2\mu}{\hbar^2}\langle H_n|\hat{H}_S+\frac{\hbar^2}{2\mu\rho^2}\left[J(J+1)-\Omega^2+\frac{3}{4}\right]-E|H_{n'}\rangle.$$

In this work, we have solved the coupled channel equations in Eq. (18) using the quasi-adiabatic log-derivative algorithm of Manolopoulos.[29]

The scattering matrix S has been extracted from the log-derivative matrix $\mathbf{Y}(\rho_i)$ at a large value of ρ_i by using the hyperspherical projection method developed in this work as an extension to previous versions.[23–25] In this method the boundary conditions are applied in Jacobi coordinates and only a single ρ sector is used, which will be described in the next subsection.

B. The hyperspherical projection method

Following Refs. 23 and 25, the asymptotic form $f_{nm}(R;J,\Omega)$ (for convenience, we have dropped the channel index) in Eq. (7) is expressed as

$$f_{nm}(R;J,\Omega)\sim k_n^{-1/2}\hat{h}_I^{(2)}(k_nR;J,\Omega)\,\delta_{nm}+k_n^{-1/2}\times\hat{h}_I^{(1)}(k_nR;J,\Omega)S_{nm}^{J\Omega}, \tag{20}$$

where $k_n=\sqrt{2\mu(E-\mathcal{E}_n^F)}/\hbar$ is the channel wave number, and $S_{nm}^{J\Omega}$ is an S matrix element. $\hat{h}_I^{(1,2)}$ are the Riccati–Hankel functions, which can be defined by the Riccati–Bessel functions $\hat{y}_I$ and $\hat{n}_I$ as[30]

$$\hat{h}_I^{(1)}(k_nR;J,\Omega)=\hat{y}_I(k_nR;J,\Omega)+i\hat{n}_I(k_nR;J,\Omega),$$
$$\hat{h}_I^{(2)}(k_nR;J,\Omega)=\hat{y}_I(k_nR;J,\Omega)-i\hat{n}_I(k_nR;J,\Omega), \tag{21}$$

and I is defined later. Using Eqs. (6) and (16) and integrating over φ, z, and θ, we have

$$h_{km}=\langle H_k(\varphi,z,\theta;i,\Omega)|\rho^{3/2}\psi_m^{J\Omega}(\rho,\varphi,z,\theta)\rangle = \rho^{1/2}\langle H_k(\varphi,z,\theta;i,\Omega)|\rho\psi_m^{J\Omega}(\rho,\varphi,z,\theta)\rangle.$$

Substituting for $|\rho\psi_m^{J\Omega}(\rho,\varphi,z,\theta)\rangle$ using Eq. (7) and inserting the asymptotic form of f_{nm} in Eq. (20) yield

$$h_{km}=\sum_n \rho^{1/2}\langle H_k(\varphi,z,\theta;i,\Omega)|f_{nm}(R;J,\Omega)|F_n(r,z,\theta;\Omega)\rangle$$
$$=\sum_n \rho^{1/2}k_n^{-1/2}\{\langle H_k(\varphi,z,\theta;i,\Omega)|\hat{h}_I^{(2)}(k_nR;J,\Omega)|\times F_n(r,z,\theta,\Omega)\rangle\delta_{nm}+\langle H_k(\varphi,z,\theta;i,\Omega)|\times\hat{h}_I^{(1)}(k_nR;J,\Omega)|F_n(r,z,\theta;\Omega)\rangle S_{nm}^{J\Omega}\}. \tag{22}$$

Taking the derivative of h_{km} with respect to ρ, we have

$$h'_{km}=\frac{\partial h_{km}}{\partial\rho}=\frac{1}{2}\rho^{-1}h_{km}+\sum_n \rho^{-1/2}k_n^{-1/2}\{\langle H_k(\varphi,z,\theta;i,\Omega)|k_nR\hat{h}_I^{(2)'}(k_nR;J,\Omega)|F_n(r,z,\theta;\Omega)\rangle\delta_{nm}+\langle H_k(\varphi,z,\theta;i,\Omega)|\times\hat{h}_I^{(2)}(k_nR;J,\Omega)r|F_n'(r,z,\theta;\Omega)\rangle\delta_{nm}+\langle H_k(\varphi,z,\theta;i,\Omega)|k_nR\hat{h}_I^{(1)'}(k_nR;J,\Omega)|F_n(r,z,\theta;\Omega)\rangle S_{nm}^{J\Omega}+\langle H_k(\varphi,z,\theta;i,\Omega)|\hat{h}_I^{(1)}(k_nR;J,\Omega)r|F_n'(r,z,\theta;\Omega)\rangle S_{nm}^{J\Omega}\}, \tag{23}$$

where

$$\hat{h}_I^{(i)'}(k_nR;J,\Omega)=\frac{\partial\hat{h}_I^{(i)}(k_nR;J,\Omega)}{\partial(k_nR)}=k_n^{-1}\frac{\partial\hat{h}_I^{(i)}}{\partial R},$$
$$F_n'(r,z,\theta;\Omega)=\frac{\partial F_n(r,z,\theta;\Omega)}{\partial r}, \tag{24}$$

and we have used the relations,

$$\frac{\partial(k_nR)}{\partial\rho}=k_nR/\rho,$$
$$\frac{\partial r}{\partial\rho}=r/\rho.$$

For simplicity, we now introduce four real matrices

$$X_{kn}^{(1)}=\rho^{1/2}\langle H_k(\varphi,z,\theta;i,\Omega)|\hat{y}_I(k_nR;J,\Omega)|F_n(r,z,\theta;\Omega)\rangle = \rho^{1/2}\int_0^{\varphi_{\max}}\int_{z_{\min}}^{z_{\max}}\int_0^{\pi}H_k^*(\varphi,z,\theta;i,\Omega)\hat{y}_I(k_nR;J,\Omega)\times F_n(r,z,\theta;\Omega)dzd\varphi\sin\theta d\theta,$$

$$X_{kn}^{(2)}=\rho^{1/2}\langle H_k(\varphi,z,\theta;i,\Omega)|\hat{n}_I(k_nR;J,\Omega)|F_n(r,z,\theta;\Omega)\rangle, \tag{25}$$

$$X_{kn}^{(3)}=\rho^{-1/2}\langle H_k(\varphi,z,\theta;i,\Omega)|k_nR\hat{y}_I'(k_nR;J,\Omega)+\tfrac{1}{2}\hat{y}_I(k_nR;J,\Omega)|F_n(r,z,\theta;\Omega)\rangle + \rho^{-1/2}\langle H_k(\varphi,z,\theta;i,\Omega)|\hat{y}_I(k_nR;J,\Omega)\times r|F_n'(r,z,\theta;\Omega)\rangle,$$

$$
\begin{aligned}
X_{kn}^{(4)} &= \rho^{-1/2}\langle H_k(\varphi,z,\theta;i,\Omega)|k_nR\hat{n}_I'(k_nR;J,\Omega)\\
&\quad + \tfrac{1}{2}\hat{n}_I(k_nR;J,\Omega)|F_n(r,z,\theta;\Omega)\rangle\\
&\quad + \rho^{-1/2}\langle H_k(\varphi,z,\theta;i,\Omega)|\hat{n}_I(k_nR;J,\Omega)\\
&\quad \times r|F_n'(r,z,\theta;\Omega)\rangle.
\end{aligned}
$$

Then, h_{km} and h_{km}' can be rewritten as

$$
\begin{aligned}
h_{km} &= \sum_n k_n^{-1/2}X_{kn}^{(1)}\delta_{nm} - i\sum_n k_n^{-1/2}X_{kn}^{(2)}\delta_{nm}\\
&\quad + \sum_n k_n^{-1/2}X_{kn}^{(1)}S_{nm}^{J\Omega} + i\sum_n k_n^{-1/2}X_{kn}^{(2)}S_{nm}^{J\Omega},\\
h_{km}' &= \sum_n k_n^{-1/2}X_{kn}^{(3)}\delta_{nm} - i\sum_n k_n^{-1/2}X_{kn}^{(4)}\delta_{nm}\\
&\quad + \sum_n k_n^{-1/2}X_{kn}^{(3)}S_{nm}^{J\Omega} + i\sum_n k_n^{-1/2}X_{kn}^{(4)}S_{nm}^{J\Omega},
\end{aligned}
\tag{26}
$$

or in matrix form

$$
\begin{aligned}
\mathbf{h} &= X^{(1)}\mathbf{k}^{-1/2}\mathbf{I} - iX^{(2)}\mathbf{k}^{-1/2}\mathbf{I} + X^{(1)}\mathbf{k}^{-1/2}S^{J\Omega}\\
&\quad + iX^{(2)}\mathbf{k}^{-1/2}S^{J\Omega},\\
\mathbf{h}' &= X^{(3)}\mathbf{k}^{-1/2}\mathbf{I} - iX^{(4)}\mathbf{k}^{-1/2}\mathbf{I} + X^{(3)}\mathbf{k}^{-1/2}S^{J\Omega}\\
&\quad + iX^{(4)}\mathbf{k}^{-1/2}S^{J\Omega}.
\end{aligned}
$$

With the definition of the log-derivative matrix $\mathbf{Y}(\rho_i)$ as $\mathbf{h}' = \mathbf{Y}(\rho_i)\mathbf{h}$,[29] we can solve these equations to obtain the *S*-matrix,

$$
S^{J\Omega}(E) = -\mathbf{k}^{1/2}\mathbf{W}^{-1}\mathbf{W}^{*}\mathbf{k}^{-1/2}, \tag{27}
$$

where

$$
\mathbf{W} = [\mathbf{Y}(\rho_i)X^{(1)} - X^{(3)}] + i[\mathbf{Y}(\rho_i)X^{(2)} - X^{(4)}], \tag{28}
$$

and $\mathbf{k}$ is a diagonal matrix with the elements $(\mathbf{k})_{n'n} = k_n\delta_{n'n}$. Equation (27) is valid for large values of ρ_i.

The order I of the Riccati–Hankel functions $\hat{h}_I^{(1,2)}$ given in Eq. (20) can be defined from the coupling matrix in Eq. (19) as

$$
I(I+1) = J(J+1) - \Omega^2 + 1. \tag{29}
$$

Thus I is usually a fractional value. In our calculations, we have taken the nearest integer value of I and ignored the resulting small error in the centrifugal potential in applying boundary conditions, whereby the more familiar spherical Bessel functions can be used. A similar treatment has been used by other groups,[20] and it has been shown that this approximation has a small effect on the magnitudes and phases of the final *S* matrix elements.

Also, we have noticed that the eigenstates of the surface Hamiltonian defined in Eq. (14) approach the asymptotic vibrational/rotational states for large ρ such that

$$
|F_n(r,z,\theta;\Omega)\rangle \approx R^{-1/2}|H_n(\varphi,z,\theta;i,\Omega)\rangle, \tag{30}
$$

$$
\mathcal{E}_n^F \approx \mathcal{E}_n^H. \tag{31}
$$

Using these relations, the matrices $\mathbf{X}^{(i)}$ in Eq. (25) can be written (for a large value of ρ),

$$
\begin{aligned}
X_{kn}^{(1)} &\approx \rho^{1/2}\langle H_k(\varphi,z,\theta;i,\Omega)|R^{-1/2}\hat{y}_I(k_nR;J,\Omega)\\
&\quad \times|H_n(\varphi,z,\theta;i,\Omega)\rangle,\\
X_{kn}^{(2)} &\approx \rho^{1/2}\langle H_k(\varphi,z,\theta;i,\Omega)|R^{-1/2}\hat{n}_I(k_nR;J,\Omega)\\
&\quad \times|H_n(\varphi,z,\theta;i,\Omega)\rangle,\\
X_{kn}^{(3)} &\approx \rho^{-1/2}\langle H_k(\varphi,z,\theta;i,\Omega)|R^{-1/2}\Bigg\{k_nR\hat{y}_I'(k_nR;J,\Omega)\\
&\quad + \frac{1}{2}\left[1+\left(\frac{r}{\rho}\right)^2\right]\hat{y}_I(k_nR;J,\Omega)\Bigg\}|H_n(\varphi,z,\theta;i,\Omega)\rangle\\
&\quad + \rho^{-1/2}\langle H_k(\varphi,z,\theta;i,\Omega)|\pm\frac{r\sqrt{R}}{\rho^2}\\
&\quad \times\hat{y}_I(k_nR;J,\Omega)|H_n'(\varphi,z,\theta;i,\Omega)\rangle,\\
X_{kn}^{(4)} &\approx \rho^{-1/2}\langle H_k(\varphi,z,\theta;i,\Omega)|R^{-1/2}\Bigg\{k_nR\hat{n}_I'(k_nR;J,\Omega)\\
&\quad + \frac{1}{2}\left[1+\left(\frac{r}{\rho}\right)^2\right]\hat{n}_I(k_nR;J,\Omega)\Bigg\}|H_n(\varphi,z,\theta;i,\Omega)\rangle\\
&\quad + \rho^{-1/2}\langle H_k(\varphi,z,\theta;i,\Omega)|\pm\frac{r\sqrt{R}}{\rho^2}\\
&\quad \times\hat{n}_I(k_nR;J,\Omega)|H_n'(\varphi,z,\theta;i,\Omega)\rangle,
\end{aligned}
\tag{32}
$$

and

$$
H_n'(\varphi,z,\theta;i,\Omega) = \frac{\partial H_n(\varphi,z,\theta;i,\Omega)}{\partial\varphi}, \tag{33}
$$

where the ''+'' and ''−'' in Eq. (32) refer to the reactant and product channels, respectively. In practice, the integrands can be integrated over the z and θ variables first. Also these integrations are only done once for a given Ω value, as they are independent of the scattering energy and J. Obviously, as a result of this approximation, we do not need to calculate the asymptotic states $\{|F_n(r,z,\theta;\Omega)\rangle\}$, which saves both CPU time and core memory. All wavefunctions and their derivatives required in Eq. (32) are computed during the propagation for the first energy point and need not be recalculated for other energies.

C. Surface functions

In the coupled-channel quantum scattering calculations, one major obstacle is to calculate the eigenstates of the surface Hamiltonian. For a multidimensional problem, it is normally the most time-consuming part since one usually diagonalizes a large coupling matrix for each step in the propagation. Although a compact basis set can be constructed by sequential diagonalization/truncation techniques, the size of the resulting basis is typically still large for a four-dimensional system.

To alleviate this difficulty, the authors have recently developed a spectral transform Krylov subspace iteration method to calculate the eigenstates of the coupling matrix.[31] It has proven highly efficient and stable in the application to the 3D RLU calculations for the $Cl+CH_4 \rightleftharpoons HCl+CH_3$ reac-

tion. In this work, we further develop this method and apply it to the 4D RBU calculations. Here, a guided spectral transform technique is suggested.

1. Guided spectral transform Lanczos method

Since the spectral transform (ST) Lanczos iteration method has been described elsewhere,[31] we only give a summary here. The algorithm consists of the conventional three-term Lanczos recurrence[32] with a Hermitian filter $F(\hat{H}_S)$

$$\beta'_{j+1}|q'_{j+1}\rangle = F(\hat{H}_S)|q_j\rangle - \alpha_j|q_j\rangle - \beta_j|q_{j-1}\rangle \tag{34}$$

with

$$\beta_1 \equiv 0, \ |q_0\rangle = 0, \tag{35}$$

and the partial reothogonalization (PRO) (Ref. 33)

$$\beta_{j+1}|q_{j+1}\rangle = \beta'_{j+1}|q'_{j+1}\rangle - \sum_{k\in\mathcal{L}(j)} \beta'_{j+1}\langle q_k|q'_{j+1}\rangle|q_k\rangle, \tag{36}$$

where $\mathcal{L}(j)$ is a collection of indices for the PRO procedure. $|q_1\rangle$ is an initial vector. The recursion coefficients α_j and β_{j+1} are the mean energy and residue of the jth vector, respectively. They define the tridiagonal matrix $\mathbf{T}_j$,

$$\mathbf{T}_j = \begin{bmatrix} \alpha_1 & \beta_2 & & & \\ \beta_2 & \alpha_2 & \beta_3 & 0 & \\ & \beta_3 & \ddots & \ddots & \\ & 0 & \ddots & \ddots & \beta_j \\ & & & \beta_j & \alpha_j \end{bmatrix}. \tag{37}$$

Diagonalizing this matrix gives the eigenvalues ϵ_n and the expansion coefficients C^n of the eigenvectors in the Krylov subspace $\{|q_k\rangle, k=1,...,j\}$ such that

$$|H_n\rangle = \sum_{k=1}^{j} C_k^n |q_k\rangle. \tag{38}$$

If the subspace is big enough to converge a set of N states of $F(\hat{H}_S)$, one can then obtain the corresponding N eigenstates of the surface Hamiltonian $\hat{H}_S$, which has the same eigenvectors but different eigenvalues $\mathcal{E}_n^H$. This is a result of the Krylov subspace being invariant under the spectral transformation performed. The eigenvalues $\mathcal{E}_n^H$ of $\hat{H}_S$ can be determined from $\epsilon_n = F(\mathcal{E}_n^H)$.

In our previous work,[31] the exponential filter $f(\hat{H}_S) = \exp[-\alpha(\hat{H}_S - H_{\min})]$ was used as $F(\hat{H}_S)$. It has been shown that this filter can be used to efficiently calculate the lowest eigenstates of $\hat{H}_S$. The action of the filter on the vectors was performed via the Chebyshev polynomials,[34]

$$f(\hat{H}_S) = \exp[-\alpha(\hat{H}_S - H_{\min})] \approx \sum_{l=0}^{L} A_l(\alpha) T_l(\hat{H}_{\text{norm}}), \tag{39}$$

where T_l denotes the lth Chebyshev polynomial, and $\hat{H}_{\text{norm}}$ the normalized operator

$$\hat{H}_{\text{norm}} = \frac{\hat{H}_S - \overline{H}}{\Delta H} \tag{40}$$

with

$$\overline{H} = \tfrac{1}{2}[H_{\max} + H_{\min}],$$

$$\Delta H = \tfrac{1}{2}[H_{\max} - H_{\min}],$$

where $H_{\max}$ and $H_{\min}$ are, respectively, estimates of the maximum and minimum eigenvalues of $\hat{H}_S$.

The expansion coefficients $A_l(\alpha)$ in Eq. (39) are determined by the following integral:

$$\begin{aligned} A_l(\alpha) &= \frac{2-\delta_{l0}}{\pi} \int_{-1}^{+1} \frac{f(E)T_l(E)}{\sqrt{1-E^2}} dE \\ &= \frac{2-\delta_{l0}}{\pi} \int_0^{\pi} e^{-\alpha\Delta H(1+\cos\theta)} \cos(l\theta) d\theta, \end{aligned} \tag{41}$$

which was evaluated by Gauss–Chebyshev quadrature.

Although the expansion in Eq. (39) converges exponentially once $l > \alpha\Delta H$, we find that it is not necessary to converge it for the calculation of eigenstates. Instead, we use the truncated polynomials as the filter in the Lanczos iteration, i.e.,

$$F(\hat{H}_S) = \sum_{l=0}^{L_G} A_l(\alpha) T_l(\hat{H}_{\text{norm}}), \tag{42}$$

where the coefficients $A_l (l > L_G)$, which have an absolute value less than 0.01 (we found that this is a good criterion for the exponential and Gaussian filters), have been excluded. L_G is much smaller than L as listed in Table I. Therefore, the efficiency of the ST Lanczos method will be enhanced significantly with this new filter as the CPU time increases approximately linearly with the number of expansion polynomials. To distinguish from the original case where the filter is calculated accurately [the residue is less than 1.0×10^{-9} in Eq. (39)], we refer to the new algorithm as the guided spectral transform (GST) Lanczos method.

The GST technique is quite general and can also be used in other fields such as the calculation of bound and resonance states of a molecule.[35] Further, the guided filter $F(\hat{H}_S)$ can be designed in terms of arbitrary functions. In quantum scattering calculations, another important filter is the Gaussian $g(\hat{H}_S) = \exp\{-[\alpha(\hat{H}_S - H_{\min})]^2\}$. Similarly, its guided filter may be chosen as

TABLE I. Comparison of the order of the Chebyshev expansion for the exponential $f(\hat{H}_S) = e^{-\alpha(\hat{H}_S - H_{\min})}$ and Gaussian $g(\hat{H}_S) = e^{-[\alpha(\hat{H}_S - H_{\min})]^2}$ filters with that for their guided filters $F(\hat{H}_S)$ defined in Eqs. (42) and (43). $H_{\min} = 0.0$ and $\alpha = 0.5$ eV^{-1} are used.

	Exponential filter		Gaussian filter	
$H_{\max}$/eV	L	L_G	L	L_G
15.0	16	6	33	9
20.0	18	7	38	10
25.0	19	7	44	11
30.0	21	8	46	12
40.0	23	9	53	14
50.0	25	9	63	15
60.0	27	10	65	16
80.0	31	11	80	18

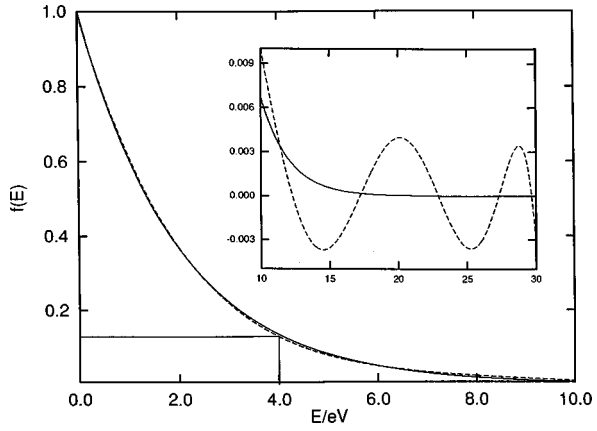

FIG. 2. The curve of the guided spectral transform (dashed line) with $L_G=8$ for the exponential function $\exp(-0.5E)$ (solid line) from $E_{\min}=0.0$ to $E_{\max}=30.0$ eV.

$$F(\hat{H}_S)=\sum_{l=0}^{L_G} B_l(\alpha)T_l(\hat{H}_{\text{norm}}) \tag{43}$$

with

$$B_l(\alpha)=\frac{2-\delta_{l0}}{\pi}\int_{-1}^{+1}\frac{g(E)T_l(E)}{\sqrt{1-E^2}}dE$$

$$=\frac{2-\delta_{l0}}{\pi}\int_0^{\pi} e^{-[\alpha\Delta H(1+\cos\theta)]^2}\cos(l\theta)d\theta. \tag{44}$$

Again, with the corresponding criterion for L_G as in Eq. (42), it is seen from Table I that the CPU time saving is substantial.

Figure 2 shows a typical curve of the GST for the exponential filter. It is clear that the approximate spectral transform well represents the profile of the exponential filter at low energies, where the curve is also *smooth* and *monotonous*. Although there are slight deviations and small waves appearing at high energies, it will not affect the calculation of the lowest eigenstates required in the quantum scattering study since the accurate eigenvalues of $\hat{H}_S$ are determined by the roots of the GST curve for obtained $F(E)$ values as shown in Fig. 2. Finding the roots is fast and can be done with several algorithms, e.g., the Newton–Raphson method.[36]

2. Evaluation of the surface Hamiltonian

As discussed above, the filter-vector multiplication in Eq. (34) is reduced to performing the action of $\hat{H}_S$ on a vector by using the Chebyshev expansion method. This $\hat{H}_S$-vector action has been carried out in a discrete variable representation (DVR) basis.

A direct product DVR basis in the variables φ, z, and θ, denoted as $\{|abc\rangle;\ a=1,...,N_\varphi,\ b=1,...,N_z,$ and $c=1,...,N_\theta\}$, has been used. $\{|a\rangle\}$ and $\{|b\rangle\}$ are the potential optimized DVRs (PO-DVRs) (Ref. 15) for φ and z, respectively. $\{|c\rangle\}$ is the primitive DVRs for the angular coordinates, whose abscissas are formed by the eigenvalues of the $\cos\theta$ operator matrix represented in a set of normalized Legendre polynomials $\{P_j(\cos\theta);\ j=|\Omega|,\ |\Omega|+1,...,N_\theta+|\Omega|-1\}$. Further, the eigenvectors define the unitary collocation matrix $\mathbf{Q}$ which transforms the wave functions between finite basis representation (FBR) and DVR in θ. In the $\{|abc\rangle\}$ basis set, the matrix representation of $\hat{H}_S$ is given by

$$[\mathbf{H}_S(\rho_i)]_{a'b'c',abc}$$
$$=[\mathbf{T}_\varphi(\rho_i)]_{a'a}\delta_{b'b}\delta_{c'c}+[\mathbf{T}_z]_{b'b}\delta_{a'a}\delta_{c'c}+\{[\mathbf{T}_\theta(z_b)]_{c'c}$$
$$+[\mathbf{T}_\Omega(\rho_i,\varphi_a)]_{c'c}\}\delta_{a'a}\delta_{b'b}+[\mathbf{V}(\rho_i)]_{a'b'c',abc}, \tag{45}$$

with

$$[\mathbf{T}_\varphi(\rho_i)]_{a'a}=\langle a'|-\frac{\hbar^2}{2\mu\rho_i^2}\frac{\partial^2}{\partial\varphi^2}|a\rangle, \tag{46}$$

$$[\mathbf{T}_z]_{b'b}=\langle b'|-\frac{\hbar^2}{2\mu_z}\frac{\partial^2}{\partial z^2}+V_{\text{ref}}(z)|b\rangle, \tag{47}$$

$$[\mathbf{T}_\theta(z_b)]_{c'c}=\sum_{j=|\Omega|}^{N_\theta+|\Omega|-1}\frac{j(j+1)\hbar^2}{2I(z_b)}\mathbf{Q}^*_{jc'}\mathbf{Q}_{jc}, \tag{48}$$

$$[\mathbf{T}_\Omega(\rho_i,\varphi_a)]_{c'c}=\sum_{j=|\Omega|}^{N_\theta+|\Omega|-1}\frac{[j(j+1)-\Omega^2]\hbar^2}{2\mu\rho_i^2\sin^2\varphi_a}\mathbf{Q}^*_{jc'}\mathbf{Q}_{jc}, \tag{49}$$

$$[\mathbf{V}(\rho_i)]_{a'b'c',abc}=[V_H(\varphi_a,z_b,\theta_c;i)-V_{\text{ref}}(z_b)]$$
$$\times\delta_{a'a}\delta_{b'b}\delta_{c'c}, \tag{50}$$

where $V_{\text{ref}}(z)$ is a reference potential in z. Thus, the action of $\hat{H}_S$ on a vector $|q\rangle=\Sigma_{abc}\psi_{abc}|abc\rangle$ can be calculated as

$$\hat{H}_S|q\rangle=\sum_{a'b'c'}\Bigg\{[\mathbf{V}(\rho_i)]_{a'b'c',a'b'c'}\psi_{a'b'c'}$$
$$+\sum_a[\mathbf{T}_\varphi]_{a'a}\psi_{ab'c'}+\sum_b[\mathbf{T}_z]_{b'b}\psi_{a'bc'}$$
$$+\sum_c[\mathbf{T}_\theta(z_{b'})]_{c'c}\psi_{a'b'c}$$
$$+\sum_c[\mathbf{T}_\Omega(\rho_i,\varphi_{a'})]_{c'c}\psi_{a'b'c}\Bigg\}|a'b'c'\rangle. \tag{51}$$

D. Differential and integral cross sections, rate constants, and tunneling

The state-to-state reaction probability for the reaction $Cl+CH_4(\nu_{3b},\nu_b,\nu_4)\rightarrow HCl(\nu)+CH_3(\nu_2,j)$ is given by

$$P^{J\Omega}_{\nu_{3b}\nu_b\nu_4\rightarrow\nu\nu_2 j}=|S^{J\Omega}_{\nu_{3b}\nu_b\nu_4\rightarrow\nu\nu_2 j}|^2, \tag{52}$$

where the vibrational quantum numbers ν, ν_{3b}, ν_b, ν_2, and ν_4 refer to the H–Cl stretch, the reactive H–C stretch, the H–CH_3 bending and the umbrella modes in CH_3 and CH_4, respectively; and j is a CH_3 rotational quantum number. The cumulative reaction probability (CRP), $N(E,J,\Omega)$, is calculated by summing the state-to-state reaction probabilities over all final and initial states, i.e.,

$$N(E,J,\Omega)=\sum_{\nu_{3b}\nu_b\nu_4}\sum_{\nu\nu_2 j}P^{J\Omega}_{\nu_{3b}\nu_b\nu_4\rightarrow\nu\nu_2 j}. \tag{53}$$

In the present work, we have not summed over the quantum numbers not explicitly treated in the reduced dimensionality calculation and thus not obtained total CRPs.

Ω-dependent differential cross sections $\sigma'^{\Omega}_{\nu_{3b}\nu_b\nu_4\rightarrow\nu\nu_2 j}(\theta_R)$ and integral cross sections $\sigma^{\Omega}_{\nu_{3b}\nu_b\nu_4\rightarrow\nu\nu_2 j}$ for going from the initial state $(\nu_{3b}\nu_b\nu_4)$ to the final state $(\nu\nu_2 j)$ are obtained from[11]

$$\sigma'^{\Omega}_{\nu_{3b}\nu_b\nu_4\rightarrow\nu\nu_2 j}(\theta_R)=\frac{1}{4k^2_{\nu_{3b}\nu_b^{\Omega}\nu_4}}\left|\sum_{J\geqslant|\Omega|}(2J+1)\times S^{J\Omega}_{\nu_{3b}\nu_b\nu_4\rightarrow\nu\nu_2 j}P_J(\cos(\pi-\theta_R))\right|^2, \tag{54}$$

$$\sigma^{\Omega}_{\nu_{3b}\nu_b\nu_4\rightarrow\nu\nu_2 j}=\frac{\pi}{k^2_{\nu_{3b}\nu_b^{\Omega}\nu_4}}\sum_{J\geqslant|\Omega|}(2J+1)P^{J\Omega}_{\nu_{3b}\nu_b\nu_4\rightarrow\nu\nu_2 j}, \tag{55}$$

where $k_{\nu_{3b}\nu_b^{\Omega}\nu_4}$ is the initial translational wave number corresponding to the vibrational state $(\nu_{3b},\nu_b^{\Omega},\nu_4)$ of CH_4 and P_J are Legendre polynomials. In Eq. (54) we have used $(\pi-\theta_R)$ in one place rather than θ_R in order to keep the definition of forward scattering consistent with the experimental convention, i.e., $\theta_R=0$ corresponds to forward scattering and $\theta_R=\pi$ to backward scattering.

The thermal rate constant is calculated from[13]

$$k(T)=\frac{Q(T)Q^{\ddagger}_{\rm rot}(T)}{2\pi\hbar Q_r(T)}\int_{-\infty}^{+\infty}dE\,\exp\{-E/kT\}N(E,J=\Omega=0), \tag{56}$$

where $Q(T)$ is the partition function at the transition state for all vibrational modes not explicitly treated in the RBU scattering calculations, $Q^{\ddagger}_{\rm rot}(T)$ is the rigid rotor symmetric top approximation for the rotational partition function of the CH_4Cl complex, $Q_r(T)$ is the reactant partition function per unit volume, and $N(E,J=\Omega=0)$ is the *CRP* evaluated for $J=0$. This treatment for $k(T)$ is equivalent to using the J and K-shifting approximations and assuming that the degrees of freedom not treated explicitly are separable.

The ground state tunneling coefficient, η^G, and transmission coefficient, κ^G, are defined as[14]

$$\eta^G=\frac{\int_{-\infty}^{+\infty}dE\,\exp\{-E/kT\}N_0(E,J=\Omega=0)}{\int_{E^*}^{+\infty}dE\,\exp\{-E/kT\}N_0(E,J=\Omega=0)}, \tag{57}$$

$$\kappa^G=\frac{1}{2kT}\exp\left\{\frac{E^*}{kT}\right\}\int_{-\infty}^{+\infty}dE\,\exp\{-E/kT\}N_0(E,J=\Omega=0), \tag{58}$$

where E^* is the vibrationally adiabatic ground state threshold energy, and N_0 is the reaction probability out of the reaction ground state summed over all product states.

The parameters and procedures employed to evaluate the partition functions defined in Eq. (56) are the same as those used in our previous 2D and 3D studies[24,25] except for setting the rotational symmetry number of CH_4 as 6 instead of 12 and that of CH_3 as 3 instead of 6. This results from the pseudoinversion symmetry discussed in Sec. II A.

III. POTENTIAL AND NUMERICAL ASPECTS

In this work, we have used the semiempirical potential energy surface given in Ref. 25. A minor modification was made to correct the reaction thermicity as the H–CH_3 bending motion is treated explicitly in the RBU model, whereby the corresponding zero point energy should no longer be included in the surface. The parameters in $V^{(2)}_{\rm CH}(R_{\rm CH})$ are set to $D_e=104.6$ kcal/mol, $\beta=1.0238\,a_0^{-1}$, and $R_e=2.0522\,a_0$. The Sato parameters in $V_{\rm LEPS}$ have been changed to $\Delta_{\rm HCl}=0.20$, $\Delta_{\rm CH}=0.25$, and $\Delta_{\rm CCl}=0.142$. For more detail, the reader is referred to Refs. 25 and 37.

This surface gives an endoergicity of 1.2 kcal/mol and a vibrationally adiabatic ground state barrier height (V_a^G) of 3.48 kcal/mol, which is in agreement with the *ab initio* (MP-SAC2) predicted values of 1.2 and 3.5 kcal/mol,[38] respectively. A late transition saddle point is obtained for the $Cl+CH_4\rightarrow HCl+CH_3$ reaction. In addition, a van der Waals minimum $ClH\cdots CH_3$ ($R_{H\cdots C}=3.6\,a_0$) with a well depth of 1.05 kcal/mol is found in the exit channel. Theoretically, Chen *et al.*[39] predicted a well depth of 0.67 kcal/mol at the level of G1 theory, while Duncan and Truong[40] obtained 2.32 kcal/mol at both the BH and HLYP and the PMP4//BH and HLYP levels. However, Duncan and Truong did not find this complex at the QCISD/6-311G(d,p) level. Thus, the existence of such a van der Waals molecule is still an interesting issue.

The coupled-channel equations are solved in hypercylindrical coordinates using the quasiadiabatic log-derivative method.[29] The surface functions were calculated by the GST Krylov subspace iteration algorithm as described above. The surface Hamiltonian was represented in a direct product DVR basis, i.e., a PO-DVR for φ and z, and a Gauss–Legendre DVR for θ. 30 Legendre basis functions were used. For the z coordinate, $N_z=25$ PO-DVR points were utilized. These were obtained by contracting 200 primitive sine-DVRs spanning the range $[-1.50, 1.75]\,a_0$ using a 1D reference potential in z. For the φ coordinate, $N_\varphi=55$ PO-DVR points were determined by contracting 200 sine-DVRs using another 1D reference potential in ϕ. Finally, a compact basis set was obtained by discarding those DVRs whose potential energies are higher than a threshold energy $V_{\rm th}=3.0$ eV.

250 adiabatic basis functions were propagated from $\rho=6.5a_0$ to $\rho=25.0a_0$ using 504 sectors. For $\Omega=0$, the 250 lowest adiabats are shown in Fig. 3. As expected, we find that the adiabats corresponding to $j=0$ or $\nu_b=0$ in the asymptotic limits are very similar to those calculated from the 3D RLU model.[25] Thus, the reaction propensities could be explained in the same way as discussed in Ref. 25. In addition, the rotational degree of freedom not only increases the spectral density at each sector, but also raises the diabats for $j>0$ substantially at $\rho<17.0\,a_0$. Therefore, it can be expected that the product would be rotationally cold.

The asymptotic analysis was performed at $\rho=25.0\,a_0$, where the S matrix elements were calculated by the hyperspherical projection method.

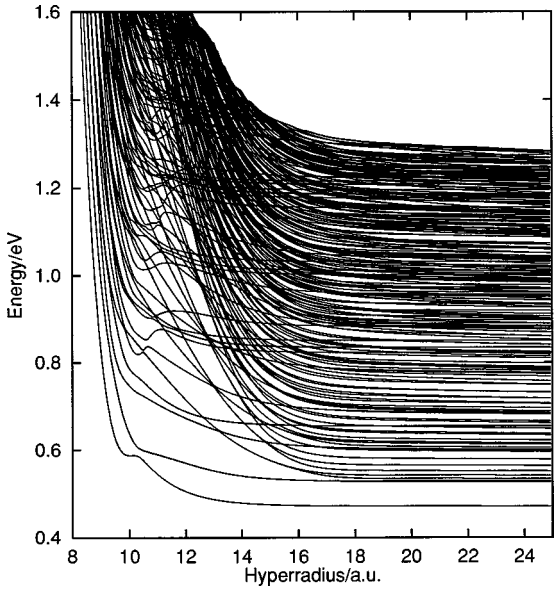

FIG. 3. Hyperspherical adiabatic energy levels for the $Cl+CH_4 \rightleftharpoons HCl+CH_3$ reaction vs the hyper-radius ρ for $\Omega=0$. The energies are relative to the bottom of the $Cl+CH_4$ potential.

IV. RESULTS AND DISCUSSION

A. Reaction probability

Figure 4 shows state-to-state reaction probabilities for the $Cl+CH_4(0,0,0) \rightarrow HCl(0)+CH_3(0,j)$ reaction as a function of energy. It can be seen that the probabilities are strongly energy-dependent and quantum resonances are observed. The largest reaction probabilities appear in the low energy range. When the energy becomes larger than 1.1 eV, the reaction probabilities tend to be small. It is also noted that the reaction probabilities for forming CH_3 in low or ground rotational states are dominant as expected from the adiabats. This can also be understood by the fact that ''Cl–H–C'' is collinear at the transition state, whereby energy transfer to the rotational mode of CH_3 is small.

Cumulative and initial vibrationally state-selected reaction probabilities are shown in Fig. 5. In the energy range below 0.75 eV, the reaction occurs only from the ground state $CH_4(0,0,0)$ since excited reactant states are not energetically accessible. However, when the total energy is higher, exicted states begin to make prominent contributions to the cumulative reaction probabilities. We also found that exciting each of the three CH_4 vibrational motions treated in the RBU model will enhance the reaction. Such enhancements have been predicted previously for the umbrella and C–H stretch vibrations.[24,25,40]

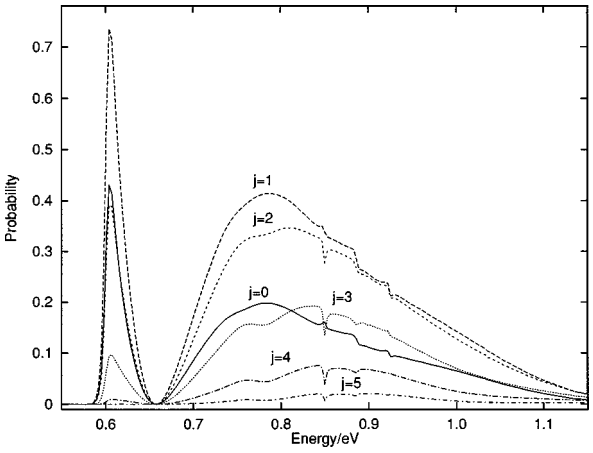

FIG. 4. State-to-state reaction probabilities vs energy, for $J=0$, for the reaction $Cl+CH_4(0,0,0) \rightarrow HCl(0)+CH_3(0,j)$ as indicated by j.

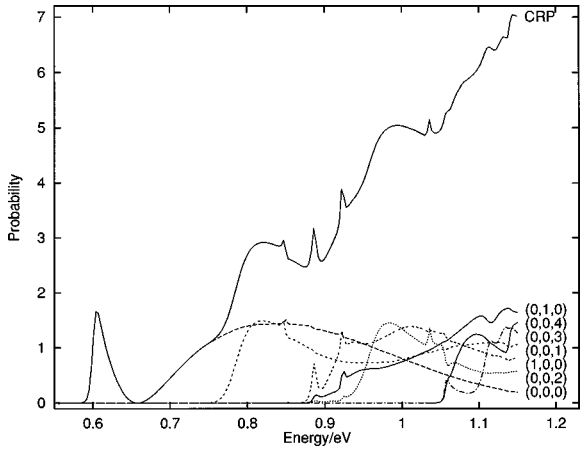

FIG. 5. Cumulative reaction probabilities (CRP) and reaction probabilities vs energy for the reaction $Cl+CH_4(\nu_{3b},\nu_b,\nu_4) \rightarrow HCl+CH_3$ summed over all product modes. The labels on the curves give the (ν_{3b},ν_b,ν_4) quantum numbers.

B. Rate constants and tunneling

Thermal rate constants have been calculated using the J and K-shifting approximations based on the total cumulative reaction probabilities for $J=0$, which are shown in Fig. 5. The calculated results are given in Table II and in Fig. 6, which also shows comparison with experimental measurements. The theoretical values are smaller than the experimental ones by 12%–45% over the temperature range 200–800 K. Thus, the agreement is good. The errors may originate from the approximate potential energy surface and/or from the reduced dimensionality treatment of the dynamics. Recently, using the dual-level direct dynamics approach and canonical variational transition state theory, Roberto-Neto *et al.*[28] have shown that the vibrationally adia-

TABLE II. Calculated thermal rate constants $[k(T)/\mathrm{cm}^3\,\mathrm{s}^{-1}\,\mathrm{molec}^{-1}]$ and ground state tunneling (η^G) and transmission (κ^G) coefficients for the $Cl+CH_4 \rightarrow HCl+CH_3$ reaction.

T/K	$k(T)$	η^G	$W(1297i)$[b]	κ^G
200	6.10(−15)[a]	13.38	4.63	2.33
250	2.46(−14)	9.90	3.32	1.59
300	6.38(−14)	7.79	2.61	1.22
350	1.29(−13)	6.33	2.18	0.99
400	2.25(−13)	5.27	1.91	0.85
500	5.23(−13)	3.85	1.58	0.68
600	9.93(−13)	3.02	1.40	0.60
800	2.59(−12)	2.16	1.23	0.52

[a]Power of 10 in parentheses.

[b]Wigner tunneling correction $[1-(h\nu/k_BT)^2/24]$ using an imaginary frequency of $1297i\ \mathrm{cm}^{-1}$.

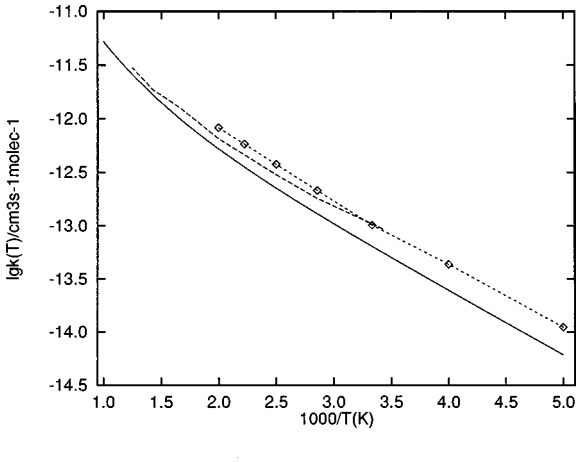

FIG. 6. Comparison of the calculated thermal rate constants (solid line) with the experimental results by Pilgrim *et al.* (Ref. 41) (dashed line) and DeMore *et al.* (Ref. 42) (squares on dashed line) for the $Cl+CH_4 \rightarrow HCl+CH_3$ reaction.

batic ground state barrier height $V_a^G = 3.5$ kcal/mol could be slightly too large for the $Cl+CH_4 \rightarrow HCl+CH_3$ reaction, which would be consistent with the present results.

It is well known that the studied reaction has a strongly nonlinear Arrhenius behavior for the temperature dependence of the absolute thermal rate constants as seen in Fig. 6. Two reasons are the spin–orbit interactions and the tunneling contribution to the hydrogen-atom abstraction. Although the electronic fine structure of Cl has been included for the reactant through the partition functions, its effects on the potential energy surface have been neglected in this work. On the other hand, the tunneling is well described in the RBU model. The pronounced tunneling effects are shown in Table II for a set of temperatures. The Wigner tunneling corrections[14] are also given for a frequency of $1297i\ cm^{-1}$, which is obtained from the potential energy surface. The Wigner factor underestimates the tunneling effect substantially as pointed out by Espinosa-García and Corchado.[43] From Table II, it is seen that the recrossing for reaction out of the ground state (η^G/κ^G) is approximately six, which partly balances the effect of tunneling on the rate constant as indicated before.[24]

For the reverse reaction, $HCl+CH_3 \rightarrow Cl+CH_4$, the calculated thermal rate constants are given in Table III together with the experimental results. The calculated values are smaller than the results of Russel *et al.*[44] by $<37\%$ and Pohjonen *et al.*[45] by $<72\%$, respectively, over the temperature range 300–500 K.

C. Differential cross sections

Zare and co-workers[46] have measured the differential cross sections for the $Cl+CH_4(\nu_{3b}=0) \rightarrow HCl(\nu=0,j')+CH_3$ and $Cl+CH_4(\nu_{3b}=1) \rightarrow HCl(\nu=0/1,j')+CH_3$ reactions, where j' is the HCl rotational quantum number, at an average translational energy of 0.159 eV. In order to compare with these experimental results, we have calculated differential cross sections at this collision energy as shown in Figs. 7, 8 and 9. Since the HCl rotational degree of freedom

TABLE III. Comparison of calculated thermal rate constants ($cm^3\ s^{-1}$ $molec^{-1}$) with the experimental results (Refs. 44,45) for the reverse, $HCl+CH_3 \rightarrow Cl+CH_4$, reaction.

T/K	PK[a]	RSSG[b]	This work
200			1.86(−14)
250			3.06(−14)
300	6.59(−14)[c]	4.78(−14)	4.14(−14)
350	1.10(−13)	6.68(−14)	5.10(−14)
400	1.61(−13)	8.59(−14)	5.98(−14)
450	2.17(−13)	1.04(−13)	6.83(−14)
500	2.75(−13)	1.22(−13)	7.69(−14)
600			9.55(−14)
800			1.43(−13)

[a]Reference 45.
[b]Reference 44.
[c]Power of 10 in parentheses.

is not treated in the RBU model, the following comparisons are made with the experimental results for $j'=0$. In the case of Fig. 9 the comparison is made with $j'=5$ which is the smallest measured j'.

Figure 7(a) shows predominantly sideways and backward scattering for $Cl+CH_4(0,0,0) \rightarrow HCl(0)+CH_3(\nu_2=0)$. It was found that the umbrella mode of the CH_3 product is not excited. These calculated results are in good agreement with the experimental measurements. In addition, Fig. 7(b) clearly demonstrates that the distributions of the rotational states of CH_3 are rather cold with $j=1$ being most probable.

Calculated differential cross sections for $Cl+CH_4(1,0,0) \rightarrow HCl(1)+CH_3(\nu_2,j)$ are shown in Figs. 8(a) and 8(b). They indicate that the excitation of the umbrella motion of CH_3 is negligible (less than 0.04%). For $\nu_2=1$, nearly equal amounts of forward and backward scat-

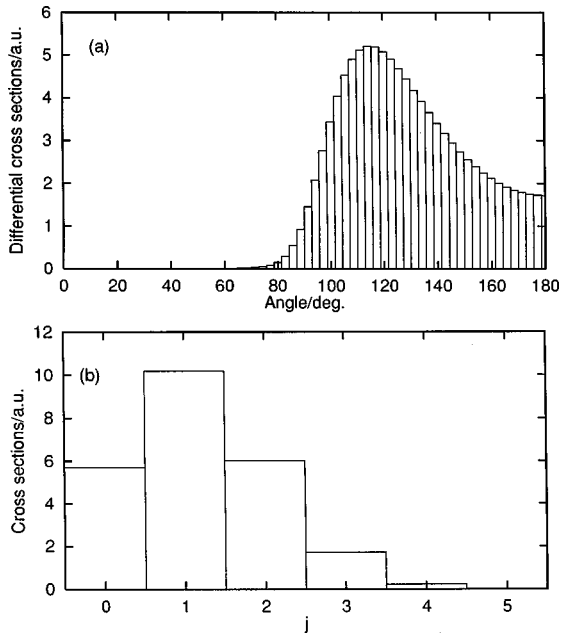

FIG. 7. (a) Differential cross sections vs angle θ_R for $Cl+CH_4(0,0,0) \rightarrow HCl(0)+CH_3(\nu_2=0)$ summed over j, at a kinetic energy 0.159 eV. $\theta_R=0$ corresponds to forward scattering. (b) Rotational state distributions of CH_3 for $Cl+CH_4(0,0,0) \rightarrow HCl(0)+CH_3(0,j)$ at a kinetic energy of 0.159 eV.

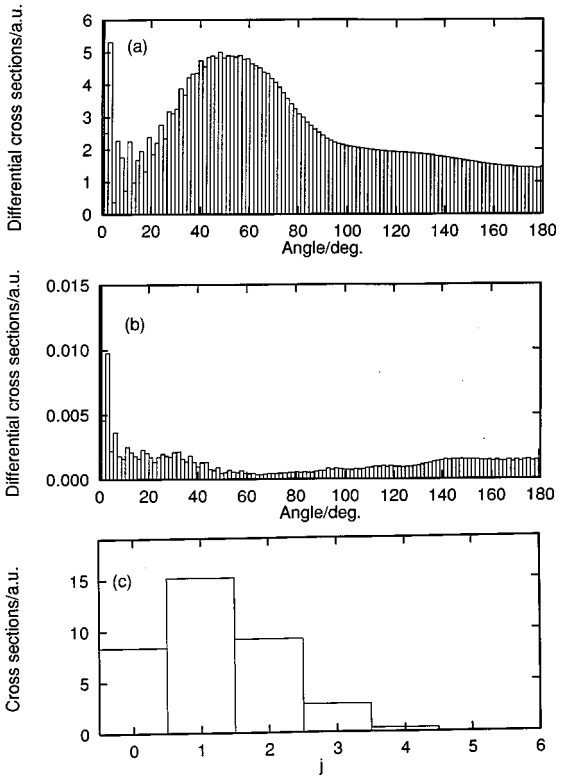

FIG. 8. (a) Differential cross sections vs angle θ_R for Cl $+CH_4(1,0,0)\rightarrow HCl(1)+CH_3(\nu_2=0)$ summed over j, at a kinetic energy 0.159 eV; (b) as in (a) but for $Cl+CH_4(1,0,0)\rightarrow HCl(1)+CH_3(\nu_2=1)$; (c) Rotational state distributions of CH_3 for $Cl+CH_4(1,0,0)$ $\rightarrow HCl(1)+CH_3(0,j)$ at a kinetic energy of 0.159 eV.

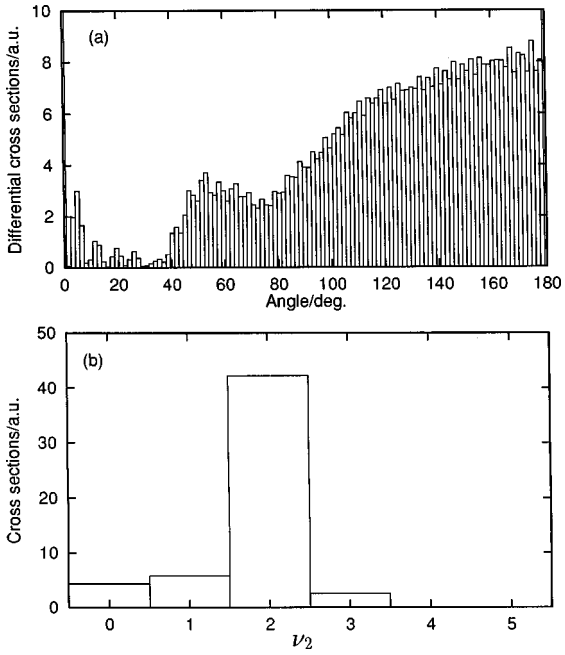

FIG. 9. (a) Differential cross sections vs angle θ_R for Cl $+CH_4(1,0,0)\rightarrow HCl(0)+CH_3$ summed over ν_2 and j, at a kinetic energy 0.159 eV; (b) Vibrational state distributions of CH_3 for Cl $+CH_4(1,0,0)\rightarrow HCl(0)+CH_3(\nu_2)$ summed over j, at a kinetic energy of 0.159 eV.

tering are obtained. However, forward and sideways scattering are dominant for $\nu_2=0$ as shown in Fig. 8(a). The CH_3 product is rotationally cold, as shown in Fig. 8(c). The calculated differential cross sections are qualitatively in agreement with the experimental results.

In Fig. 9(a), calculated differential cross sections are shown for $Cl+CH_4(1,0,0)\rightarrow HCl(0)+CH_3$. The products are predominantly scattered in the backward hemisphere, which is consistent with the experimental measurements. Figure 9(b), however, shows that the umbrella motion of CH_3 has been significantly excited, with $\nu_2=2$ being most probable, while the experiments indicate no, or only small vibrational excitation. This discrepancy has been discussed in our previous work.[25]

V. CONCLUSIONS

A four-dimensional state-to-state reactive quantum scattering model, termed the rotating bond umbrella (RBU) model, has been developed and applied to the Cl $+CH_4\rightleftharpoons HCl+CH_3$ reaction based on an empirical potential energy surface. Time-independent scattering calculations have been performed in hypercylindrical coordinates using a quasiadiabatic log-derivative algorithm. Boundary conditions have been applied using a single ρ-sector hyperspherical projection method, which was developed in this work.

A guided spectral transform Krylov subspace iteration method has been developed and used to find the eigenvalues and eigenvectors of the coupling matrix appearing in the coupled channel equations. This algorithm allows us to use a large basis set and it was found to be stable and efficient in this 4D RBU study of the $Cl+CH_4$ reaction.

Reaction probabilities, thermal rate constants and tunneling have been studied. A pronounced tunneling effect has been obtained. It was found that the CH_3 product is rather rotationally cold. The calculated rate constants for both the forward and the reverse reactions are smaller than the experimental results, but the agreement is fairly good.

State-to-state differential cross sections for $CH_4(0,0,0)$ and $CH_4(1,0,0)$ to form HCl in the vibrational ground and first excited states were investigated in detail at a kinetic energy of 0.159 eV. Our calculated results are in overall agreement with the available experimental observations. For $Cl+CH_4(0,0,0)\rightarrow HCl(0)+CH_3$, the calculated differential cross sections give sideways scattering in the backward hemisphere without vibrational excitation of the methyl. For the $Cl+CH_4(1,0,0)\rightarrow HCl(1)+CH_3$ reaction, there is predominantly forward and sideways scattering. The excitation of the umbrella mode of the methyl is negligible. Also for $Cl+CH_4(1,0,0)\rightarrow HCl(0)+CH_3$ are our calculated differential cross sections in overall agreement with the measurements, i.e., the products are mainly backward scattered. However, in this case we obtain the methyl radical substantially excited in contrast to the experimental results.

Finally, it would be highly desirable to have a more accurate potential energy surface and also to include the rotational degree of freedom of HCl in the dynamical calculations in order to achieve a more detailed comparison with experiments.

ACKNOWLEDGMENTS

The calculations were performed on a Silicon Graphics Power Challenge supercomputer at Chalmers University of Technology and Göteborg University. This research has been supported by the Swedish Natural Science Research Council (NFR), the Swedish Council for Planning and Coordination of Research (FRN) and the Wallenberg Foundation.

[1] G. C. Schatz and A. Kuppermann, J. Chem. Phys. **65**, 4668 (1976).
[2] D. C. Clary, Science **279**, 1879 (1998); J. Phys. Chem. **98**, 10678 (1994).
[3] S. K. Pogrebnya, J. Echave, and D. C. Clary, J. Chem. Phys. **107**, 8975 (1997).
[4] U. Manthe, T. Seideman, and W. H. Miller, J. Chem. Phys. **99**, 10078 (1993); **101**, 4759 (1994); U. Manthe and F. Matzkies, Chem. Phys. Lett. **282**, 442 (1998).
[5] D. Neuhauser, J. Chem. Phys. **100**, 9272 (1994).
[6] J. Z. H. Zhang, J. Dai, and W. Zhu, J. Phys. Chem. A **101**, 2746 (1997); D. H. Zhang and J. Z. H. Zhang, J. Chem. Phys. **101**, 1146 (1994); **100**, 2697 (1994); **99**, 5615 (1993); W. Zhu, J. Z. H. Zhang, Y. C. Zhang, Y. B. Zhang, L. X. Zhan, S. L. Zhang, and D. H. Zhang, *ibid.* **108**, 3509 (1998); W. Zhu, J. Q. Dai, J. Z. H. Zhang, and D. H. Zhang, *ibid.* **105**, 4881 (1996); W. Zhu, J. Z. H. Zhang, and D. H. Zhang, Chem. Phys. Lett. **292**, 46 (1998).
[7] D. H. Zhang and J. C. Light, J. Chem. Phys. **104**, 4544 (1996); **105**, 1291 (1996); D. H. Zhang, J. C. Light, and S.-Y. Lee, *ibid.* **109**, 79 (1998).
[8] Q. Sun and J. M. Bowman, J. Chem. Phys. **92**, 1021,5201 (1990); Int. J. Quantum Chem. **23**, 115 (1989).
[9] A. N. Brooks and D. C. Clary, J. Chem. Phys. **92**, 4178 (1990).
[10] D. C. Clary, J. Chem. Phys. **95**, 7298 (1991); Chem. Phys. Lett. **192**, 34 (1992).
[11] G. Nyman and D. C. Clary, J. Chem. Phys. **100**, 3556 (1994).
[12] T. Takayanagi and G. C. Schatz, J. Chem. Phys. **106**, 3227 (1997).
[13] G. Nyman and D. C. Clary, J. Chem. Phys. **99**, 7774 (1993); D. C. Clary, G. Nyman, and R. Hernandez, *ibid.* **101**, 3704 (1994); G. Nyman and D. C. Clary, *ibid.* **101**, 5756 (1994); G. Nyman, D. C. Clary, and R. D. Levine, Chem. Phys. **191**, 223 (1995).
[14] G. Nyman, J. Chem. Phys. **104**, 6154 (1996); Chem. Phys. Lett. **240**, 571 (1995).
[15] J. Echave and D. C. Clary, J. Chem. Phys. **100**, 402 (1994).
[16] J. M. Bowman and D. Wang, J. Chem. Phys. **96**, 7852 (1992); D. Wang and J. M. Bowman, *ibid.* **96**, 8906 (1992); **98**, 6235 (1993).
[17] D. Wang and J. M. Bowman, J. Chem. Phys. **101**, 8646 (1994).
[18] H. Szichman, I. Last, and M. Baer, J. Phys. Chem. **97**, 6436 (1993); **98**, 828 (1994).
[19] N. Balakrishnan and G. D. Billing, J. Chem. Phys. **101**, 2785 (1994).
[20] R. B. Walker and E. F. Hayes, in *The Theory of Chemical Reaction Dynamics* (Reidel, Dordrecht, 1986), p. 105.
[21] D. K. Bondi and J. N. L. Connor, Chem. Phys. Lett. **92**, 570 (1982).
[22] R. T. Pack and G. A. Parker, J. Chem. Phys. **87**, 3888 (1987).
[23] E. F. Hayes, P. Pendergast, and R. B. Walker, *Advances in Molecular Vibrations and Collision Dynamics* (JAI, Greenwich, 1994), Vol. 2A.
[24] G. Nyman, H. G. Yu, and R. B. Walker, J. Chem. Phys. **109**, 5896 (1998).
[25] H. G. Yu and G. Nyman, Phys. Chem. Chem. Phys. **1**, 1181 (1999).
[26] J. Römelt, Chem. Phys. Lett. **74**, 263 (1980); A. Kuppermann, J. A. Kaye, and J. P. Dwyer, *ibid.* **74**, 257 (1980); J. Echave, J. Chem. Phys. **104**, 1380 (1996).
[27] R. Atkinson, D. L. Baulch, R. A. Cox, R. F. Hampson, Jr., J. A. Kerr, and J. Troe, J. Phys. Chem. Ref. Data **21**, 1125 (1992).
[28] O. Roberto-Neto, E. L. Coitiño, and D. G. Truhlar, J. Phys. Chem. A **102**, 4568 (1998).
[29] D. E. Manolopoulos, J. Chem. Phys. **85**, 6425 (1986); D. E. Manolopoulos, M. D'Mello, and R. E. Wyatt, *ibid.* **91**, 6096 (1989).
[30] J. J. Sakurai, *Modern Quantum Mechanics* (Addison–Wesley, New York, 1994).
[31] H. G. Yu and G. Nyman, Chem. Phys. Lett. **298**, 27 (1998).
[32] C. Lanczos, J. Res. Natl. Bur. Stand. **45**, 255 (1950).
[33] H. D. Simon, Math. Comput. **42**, 115 (1984).
[34] H. Tal-Ezer and R. Kosloff, J. Chem. Phys. **81**, 3967 (1984); R. Kosloff and H. Tal-Ezer, Chem. Phys. Lett. **127**, 223 (1986).
[35] H. G. Yu and G. Nyman, J. Chem. Phys. (submitted).
[36] W. H. Press, S. A. Teukolsky, W. T. Vetterling, and B. P. Flannery, *Numerical Recipes* (Cambridge University Press, Cambridge, 1986).
[37] R. J. Duchovic, W. L. Hase, and H. B. Schlegel, J. Phys. Chem. **88**, 1339 (1984); W. H. Hase, S. L. Mondro, R. J. Duchovic, and D. M. Hirst, J. Am. Chem. Soc. **109**, 2916 (1987).
[38] T. N. Truong, D. G. Truhlar, K. K. Baldridge, M. S. Gordon, and R. Stecker, J. Chem. Phys. **90**, 7137 (1989).
[39] Y. Chen, E. Tschuikow-Roux, and A. Rauk, J. Phys. Chem. **95**, 9832 (1991).
[40] W. T. Duncan and T. N. Truong, J. Chem. Phys. **103**, 9642 (1995); **109**, 3703 (1998).
[41] J. S. Pilgrim, A. McIlory, and C. A. Taatjes, J. Phys. Chem. A **101**, 1873 (1997).
[42] W. B. DeMore *et al.*, JPL *publications* 92-20, Jet Propulsion Laboratory, 1992.
[43] J. Espinosa-García and J. C. Corchado, J. Chem. Phys. **105**, 3517 (1996).
[44] J. J. Russel, J. A. Seetula, S. M. Senkan, and D. Gutman, Int. J. Chem. Kinet. **20**, 759 (1988).
[45] M.-L. Pohjonen and J. Koskikallio, Acta Chem. Scand. **33**, 449 (1979).
[46] A. J. Orr-Ewing, W. R. Simpson, T. P. Rakitzis, S. A. Kandel, and R. N. Zare, J. Chem. Phys. **106**, 5961 (1997); W. R. Simpson, A. J. Orr-Ewing, T. P. Rakitzis, S. A. Kandel, and R. N. Zare, *ibid.* **103**, 7299 (1995); W. R. Simpson, T. P. Rakitzis, S. A. Kandel, A. J. Orr-Ewing, and R. N. Zare, *ibid.* **103**, 7313 (1995); W. R. Simpson, T. P. Rakitzis, S. A. Kandel, T. Lev-On, and R. N. Zare, J. Phys. Chem. **100**, 7938 (1996); A. J. Orr-Ewing and R. N. Zare, Annu. Rev. Phys. Chem. **45**, 315 (1994); W. R. Simpson, A. J. Orr-Ewing, and R. N. Zare, Chem. Phys. Lett. **212**, 163 (1993).